ChemCatChem

Research Article
doi.org/10.1002/cctc.202300778

Chemistry Europe
European Chemical Societies Publishing

www.chemcatchem.org

Peptide-based Organocatalyst on Stage: Functionalizing Mesoporous Silica by Tetrazine-Norbornene Ligation

Raoul D. Brand[+],[a] Steffen A. Busche[+],[b] Hans G. Börner,*[b] and Bernd M. Smarsly*[a]

Organocatalysis via the enamine mechanism developed to one of the most relevant tools in carbonyl chemistry and is widely used in asymmetric organic synthesis. In this work, a strategy is presented to conveniently immobilize a peptide-based catalyst on silica supports for use in continuous flow catalysis reactions. A set of different porous silica supports is investigated spanning from mesoporous silica particles with defined pore sizes suitable for packed bed column reactors to silica monoliths with hierarchical meso-macropore spaces. While the silica supports are functionalized with norbornene entities, the peptide-based organocatalyst is modified with a tetrazine moiety, enabling the immobilization via inverse electron-demand Diels-Alder (IEDDA) reaction. The ligation results in catalyst loadings up to 0.2 mmol g^{-1}, without compromising the mesopore network. The catalytic activity of the materials is proven by the asymmetric C–C coupling reaction of *n*-butanal to ß-nitrostyrene proceeding in high yield and enantioselectivity in both batch and continuous flow setups.

Introduction

The field of organocatalysis, which received additional attention in 2021 with the Nobel Prize in Chemistry awarded to Benjamin List and David MacMillan, has significantly expanded the toolbox for stereoselective fine chemical synthesis.[1] Proline catalysis and the enamine mechanism have served as an exciting prototype of the capabilities of organocatalysts, which have found wide application in asymmetric synthesis.[2] Recently, the scope of catalysts has been broadened by extending the catalytic unit to more complex motifs such as oligopeptides.[3] Wennemers *et al.* introduced the tripeptide motif H-D-Pro-Pro-Glu-NH_2 that was selected by combinatorial means and proved significant benefits in productivity, giving excellent results in a stereoselective addition reaction of aldehydes and nitro olefins.[4–6] The peptide has already been successfully used in heterogeneous catalysis by supporting on 1% cross-linked polystyrene microgel resins applied under continuous flow conditions.[6,7]

However, the material family of silica-based stationary phases offers tailored hierarchical pore systems, durable surface areas independent of the solvent and establishes interface modification chemistries that might contribute not only to the catalyst performance, but also to the reusability and sustainability of organocatalysts.[8] For instance, a proline derived catalyst supported on silica and its use in water as a green solvent has also been reported.[9] Applying these heterogeneous catalyst materials to continuous flow reactors offers additional advantages such as increased safety, higher energy efficiency, a homogeneous temperature across the reactor, and an easier scale up process.[10]

In general, silica has proven to be a suitable support material due to chemical inertness, high mechanical durability, as well as the possibility to rationally design the pore space on different levels and readily modify the silanol-containing interfaces.[11] While silica-based materials constitute a rich and diverse material family, two major classes have been identified as particularly suitable for catalyst supports in flow chemistry applications: monolithic silica as introduced by Nakanishi *et al.* possesses hierarchical pore systems in which the macropores ensure mass flow through the reactor and low back pressures, while the mesopores provide a high surface area for functionalization.[12] In regard to mass transport, these meso-macroporous monoliths feature beneficial hydraulic permeability as well as moderate diffusion mass transfer resistance within the mesoporous domains. One major feature of this material lies with the deliberate control of the mesopore and macropore dimensions, independently from each other.[13] As a consequence, this class of material is studied in regards to applications in flow catalysis, where, through modifications of the sol gel synthesis, the pore morphology might be tailored to specific reactions. Next to silica monoliths, packed bed column reactors filled with mesoporous silica particles of uniform spherical shape offer adequate flow properties, and enable a

[a] R. D. Brand,[+] Prof. Dr. B. M. Smarsly
Institute of Physical Chemistry
Justus-Liebig-University Giessen
Heinrich-Buff-Ring 17
35392 Giessen (Germany)
E-mail: bernd.smarsly@phys.chemie.uni-giessen.de

[b] S. A. Busche,[+] Prof. Dr. H. G. Börner
Department of Chemistry
Humboldt-University of Berlin
Brook-Taylor-Str. 2
12489 Berlin (Germany)
E-mail: h.boerner@hu-berlin.de

[+] These authors contributed equally to this work.

Supporting information for this article is available on the WWW under https://doi.org/10.1002/cctc.202300778

suitable alternative for flow catalysis. As those are the base of commonly used chromatography phases, such silica particles, being optimized for homogeneous packing, are commercially available.

To equip silica supports with oligopeptides and introduce complex functionalities at the surfaces, material-specific non-covalent coatings e.g. by selected peptide-based adhesive domains or covalent attachment strategies are available.[14] For flow catalysis, the latter offers obvious advantages as permanent anchoring largely prevents catalyst wash-off, and highly effective orthogonal ligation chemistries can be employed to attach the peptide entities in a selective manner.[15] Among other strategies, relying for instance on metal catalyzed Huisgen 1,3-dipolar cycloadditions, Staudinger coupling, thiol-ene or thiol-quinone Michael additions, or strain-promoted 1,3-cycloadditions, the ligation of (a)symmetric 1,2,4,5-tetrazines with *trans*-cyclooctene moieties proved to proceed fast and cleanly via an inverse electron-demand Diels-Alder mechanism (IEDDA).[16] While the bio-orthogonal, catalyst-free and ultrafast IEDDA of tetrazines and *trans*-cyclooctenes has found applications in fields of molecular biology and biomedicine, e.g. for DNA labeling or targeted nuclear imaging, the use of this effective coupling method in materials synthesis is just at the onset to be fully explored.[17] However, the advent of cost effective IEDDA alternatives, relying on asymmetric tetrazines and inexpensive norbornene derivatives provides opportunities for profound use in materials synthesis, e.g. polymer segment coupling and DNA modification.[18,19]

Here we adapt the IEDDA coupling for the functionalization of silica supports with a peptide-based organocatalyst (Figure 1). The comparative study uses two different types of silica support materials, such as monolithic silica possessing mesopores and macropores, as well as defined mesoporous silica particles of discrete sizes. The catalytically active tripeptide H-D-Pro-Pro-Glu-NH_2 was loaded onto the silica carriers and the activity and selectivity were studied in a model reaction, to prove availability and accessibility of pore systems as well as stability of the support-catalyst constructs.

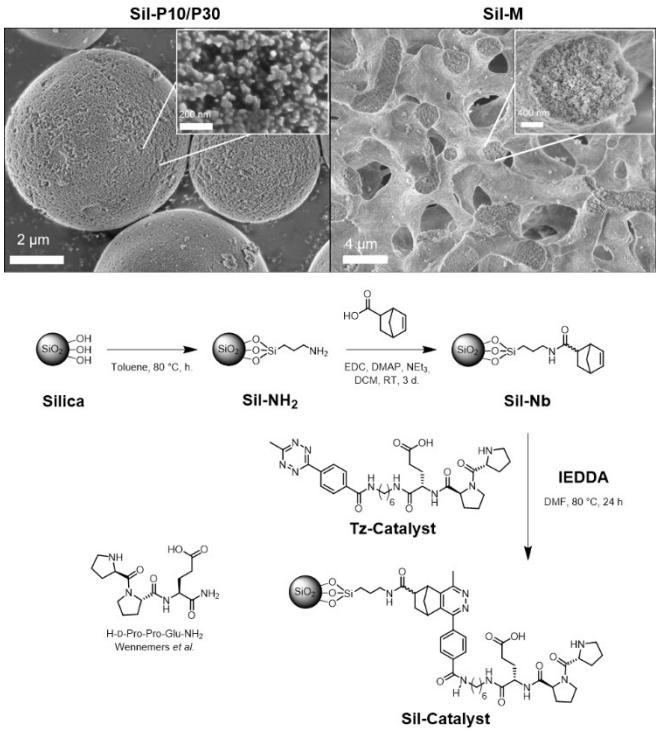

Figure 1. Silica supports (top) and schematic functionalization strategy (bottom). SEM images (top) of porous silica particles (left) and a hierarchical porous silica monolith (right) with the mesopore structure visible in the zoomed inlets and functionalization route (bottom) employing silica surface modification and subsequent IEDDA ligation to introduce the peptide-based organocatalyst.

Results and Discussion

Silica carrier supports

Heterogeneous organocatalysis requires space for solvatization and conformational flexibility, but also accessibility of catalytic sites for starting materials and drainage of products. In case of rigid, non-dynamic supports such as mesoporous silica, in comparison to swellable polystyrene microgel supports based on 1%-divinylbenzene-crosslinked polystyrene, permanently active surfaces are present.[20] Thus, the porous structure defines not only the active surface but also critical transport dynamics within the materials. As supports, two different materials of commercial porous silica particles were chosen, featuring mesopore diameters of either 10 nm or 30 nm (Sil-P10 and Sil-P30), to investigate the impact of the mesopore sizes on the catalytic performance in packed bed flow reactors. Apart from these, also monolithic silica possessing mesopores and macropores with average pore dimensions of 3–10 nm and 4 µm, respectively, were used (Sil-M, Figure 1). Both the particles and the monolithic materials meet typical porosity parameters, being suitable for the application in HPLC and performed well in previous studies on organocatalysis, using classical, non-peptidic catalysts such as propylamine or 4-(dimethylamino) pyridine (DMAP).[21,22]

Silica functionalization and introduction of the peptide catalyst

Due to ease of processability and straightforward characterization, the spherical silica particles with a mean pore diameter of 30 nm (Sil-P30) were chosen to optimize the functionalization method (Figure 1). Sil-P30 occurs as a powder material, making purification and isolation throughout the multi-step synthesis feasible. Additionally, the comparatively large mesopore volume was assumed to be more suitable for the immobilization of the spacious peptide catalyst compared to Sil-P10 to reduce diffusion limitations during the functionalization.

The silica surface was modified by condensation reaction of the surface silanol groups with (3-aminopropyl)trimethoxysilane (APTMS) to immobilize propylamine groups. To these, 5-norbornene-2-carboxylic acid as *endo*-/*exo*-mixture was coupled

with *N*-(3-di-methylaminopropyl)-*N*-ethylcarbodiimide hydrochloride (EDC) and DMAP, giving the ene-component required to proceed the IEDDA peptide ligation.[23] The optimized conditions were used to functionalize the Sil-P10 and Sil-P30 particles as well as the Sil-M monolith. The tetrazine functional H-D-Pro-Pro-Glu-NH_2 (Tz-Catalyst) counterpart was accessed by solid-phase supported peptide synthesis on a hexamethylene-diamine preloaded 2-chlorotrityl chloride resin.[24,25] This allows the fully protected peptide H-D-Pro-Pro-Glu-NH-$(CH_2)_6NH_2$ to be released from the resin with an amine-functional C-terminus.[26] In a subsequent solution reaction, the C-terminal functionality reacted with an *N*-hydroxysuccinimide active ester of an asymmetric 1,2,4,5-tetrazine (4-(6-methyl-1,2,4,5-tetrazin-3-yl)-benzoic acid, Tz-COOH). The desired Tz-Catalyst could be isolated after deprotection with trifluoroacetic acid (TFA) in a clean manner.[27,28]

The asymmetric tetrazine entity has a methyl substituent in *para*-position, which profoundly stabilizes the tetrazine, making it more thermally stable and tolerant against peptide deprotection conditions, but decreasing the reactivity compared to the unsubstituted analogue.[19,29] However, the immobilization of the Tz-Catalyst by IEDDA coupling with the silica anchored norbornene derivative is straightforward at elevated temperatures. The conversion of the pink Tz to colorless pyridazine products can be monitored with UV-Vis spectroscopy at $\lambda_{max} =$ 538 nm. The homogeneous model ligation of Tz-COOH (1.00 eq.) and Nb-COOH (1.60 eq.) follows a pseudo-1st-order reaction type at reaction temperatures of 80 °C in DMF, and the Tz moiety proved stability under these conditions.[19,30–32]

Figure 2 shows that the homogeneous reaction of two amid analogues Tz-CONHEt and Nb-CONHEt (60 min) proceeds quantitatively with rather comparable rates as the acid precursor (40 min). When using the bulkier Tz-Catalyst, the time increased to 140 minutes. As expected, the heterogeneous ligation of Tz-CONHEt and Nb-functionalized Sil-P10/30-Nb particles proceeds significantly more slowly. It is interesting that both ligations are complete after 240 min despite different pore sizes. This indicates that the accessibility of the norbornene moiety attached to the silica surface is not limited by different pore sizes for the IEDDA reaction. However, a lower Tz concentration (3.63 mg mL^{-1}) had to be used to properly suspend the silica particles, which then also affected the reaction rates. Still, it can be deduced that, while the immobilized norbornene reacts more slowly, a complete conversion can be achieved after longer reaction times.

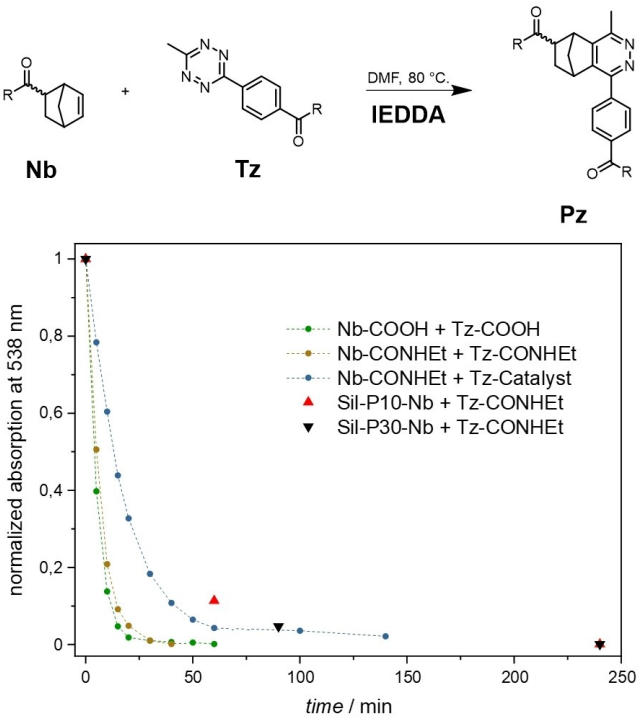

Figure 2. UV-Vis kinetics of the IEDDA reaction of different norbornenes Nb and tetrazines Tz to the pyridazine products Pz (small molecules vs. Sil-P10/30-Nb). [Conditions]: Nb (1.60 eq.), Tz (1.00 eq., 20 mg mL^{-1}), DMF, 80 °C; Sil-P–Nb (1.00 eq.), Tz (1.00 eq., 3.63 mg mL^{-1}), DMF, 80 °C.

Characterization of the functionalized materials

The different silica supports were intensively characterized at each of the modification steps through argon physisorption (nitrogen physisorption in case of the monolithic samples because of the higher sample throughput), infrared spectroscopy and elemental analysis, to couple insights into chemical modification with changes in surface area and porosity. The argon physisorption isotherms (Figure 3) of the unfunctionalized carrier materials all exhibit a type IV pattern featuring a hysteresis loop typical of mesoporous silica materials of this kind.[33] Because of the relatively large mesopore sizes of the Sil-P30 particles (Figure 3, top row), the filling of the pores occurs at large relative pressures and the narrow hysteresis loop indicates that pore blocking effects are absent. The materials with smaller mesopore sizes (Sil-P10 particles (Figure 3, middle row) and Sil-M monolith (Figure 3, bottom row)) show a slightly different isotherm, where the increase in adsorbed volume is shifted towards smaller relative pressures. Additionally, the delayed desorption, presumably caused by pore blocking effects, induces the hysteresis loops to broaden significantly in case of the monolith. Upon functionalization, a stepwise decrease in the adsorbed volume can be noticed for each material (Figure 3, left row), as the immobilized species continues to occupy more space inside the mesopores. This effect is also visualized in the pore size distribution, where the strong decrease in the cumulative pore volume can be attributed to the catalyst preferably taking up space inside the larger mesopores, while the very small mesopores appear to be unaffected, presumably due to diffusion limitations. These results appear even more pronounced in the data given by the samples with smaller mesopores (Sil-P10 and Sil-M), where the cumulative pore volume after the last functionalization step is reduced to only around 30% compared to the unfunctionalized material. While each step is similarly followed by a strong decrease in adsorbed volume, the shape of the isotherm remains largely the same, meaning the pore network is not compromised upon functionalization. Indeed, the appearance

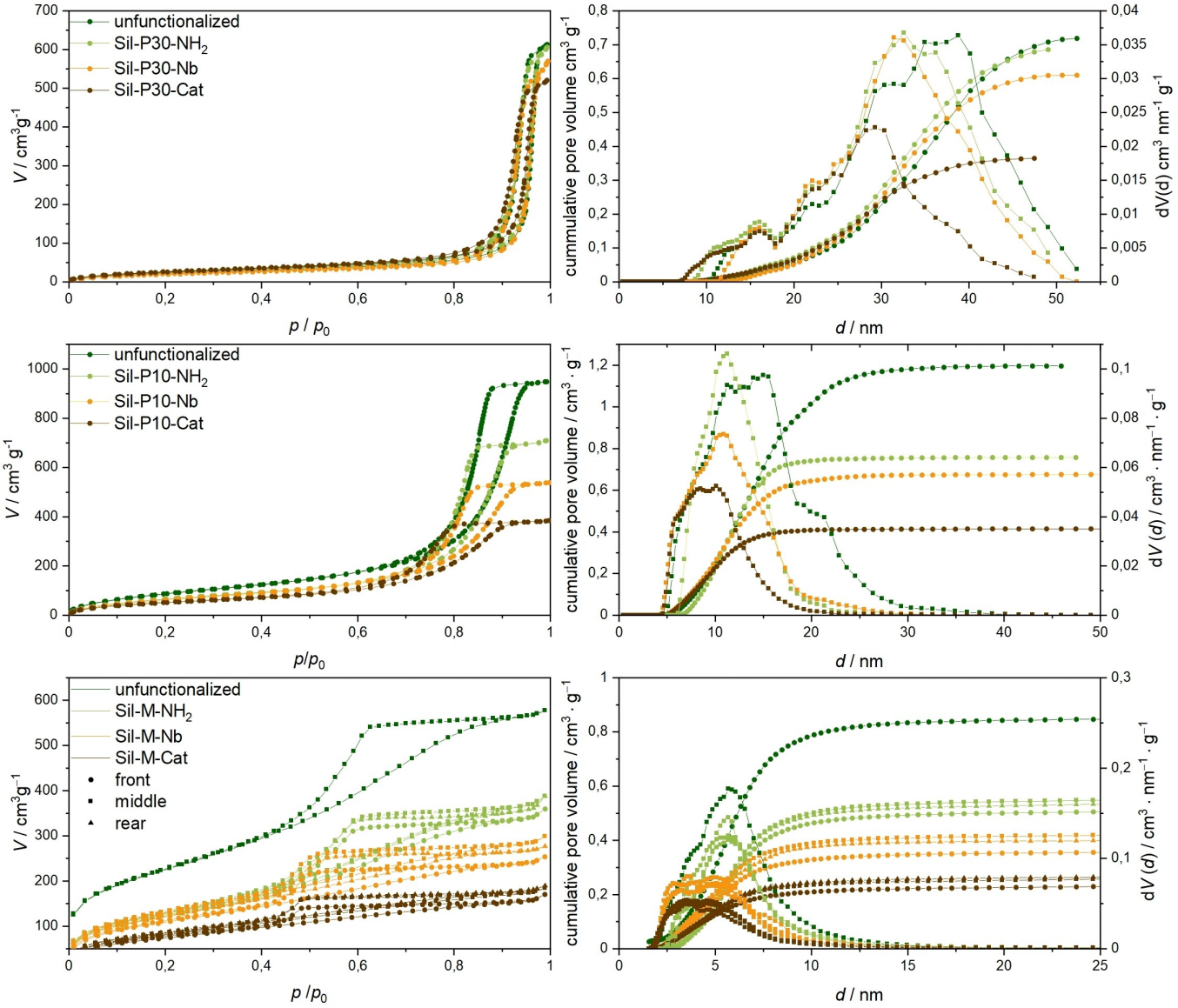

Figure 3. Ar-Physisorption isotherms (left) and pore size distributions (right) for each functionalization step of Sil-P30 (top row), Sil-P10 (middle row) and N_2-Physisorption of Sil-M (bottom row).

suggests a homogeneous distribution of the catalyst inside the pore system, with no separate inaccessible pore populations. Considering the relatively small mesopore sizes as well as the sterically demanding tripeptide, these findings are encouraging, as the functionalization appears not to be hindered significantly by diffusion limitations. Functionalization of monolithic silica is recognized to be more challenging compared to silica particles. This originates from the fact that modification mixture and concentration might locally differ radially and length wise, which requires particular care during analysis. For the measurement of the silica monolith, three samples of the front, middle and rear part were analyzed separately. While all parts appear to be successfully functionalized with the tripeptide, a slight degree of inhomogeneity can be seen comparing the three parts of each step. The isotherms of the front parts are shifted towards lower adsorbed volumes, indicating a slightly higher catalyst loading compared to the rest of the monolith. The calculated BET surface areas and pore volumes of each material are listed in the Supporting Information (*Table S1*).

In general, physisorption data suggests a covalent and quite homogeneous functionalization of the pore space for all silica materials. While the pore volume decreases dramatically upon introduction of the sterically demanding tripeptide, the pore network appears to remain intact in all samples, including that of the silica monolith which possesses the smallest mesopores. Additionally, the materials were studied by diffuse reflectance infrared Fourier transform spectroscopy (DRIFTS, Figure 4). Upon amine functionalization with APTMS, vibrational bands at 2940 cm^{-1} can be identified that correspond to the CH stretching modes of the propyl moiety, accompanied by the weak vibrational band of the NH stretching bond around 3300 cm^{-1}. After the norbornene coupling, another band at

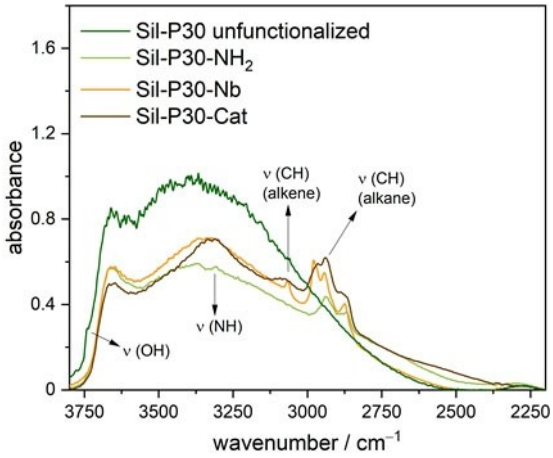

Figure 4. Excerpt of the DRIFT spectra of Sil-P30 after each functionalization step. (Complete spectra can be found in the supporting information.)

3069 cm^{-1} can be assigned to the CH stretching mode of the alkene (see SI *Figure S1* for the complete DRIFT spectra). When compared to the unfunctionalized material, the intensity of the OH stretching bond (3740 cm^{-1}) of the surface silanol groups is notably diminished upon functionalization.

As another method to confirm the presence of the catalyst on the material, thermogravimetric analysis supported by mass spectrometry was applied. Figure 5 shows the weight loss of Sil-P30-Cat upon heating to 800 °C (see SI *Figure S2* for Sil-P10-Cat). A first decrease can be noticed around 100 °C which can be assigned to the loss of adsorbed water on the silica network, as confirmed by the mass spectrometry data, showing an increase of the signal with m/z ratio of 18 corresponding to the molecular mass of H_2O. At around 300 °C and 500 °C, additional weight loss is caused by the release of nitrogen oxides (m/z = 30, NO; m/z = 46, NO_2) and carbon dioxide (m/z = 44, CO_2), which indicates the presence of an organic species incorporated into the silica matrix. The combined weight loss is approx-

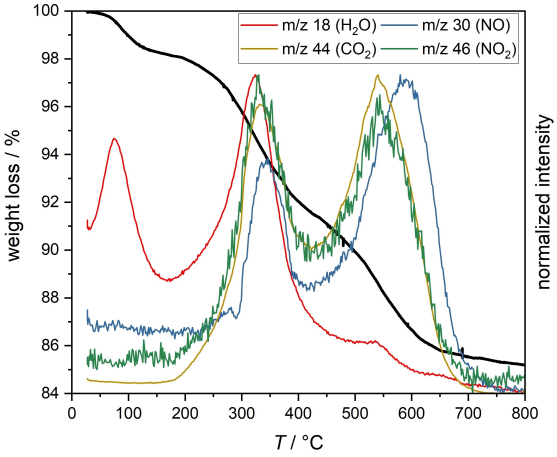

Figure 5. Thermogravimetric analysis of Sil-P30-Cat showing the weight loss upon heating (black curve) and the normalized intensity of the detected mass to charge ratios corresponding to the molecular mass of selected oxides.

Table 1. NH_2 or catalyst loadings of the amino and functionalized materials as determined by elemental analysis based on nitrogen content.

Material	NH_2/mmol g^{-1}	Catalyst loading/mmol g^{-1}
Sil-P30	0.40	0.09
Sil-P10	1.60	0.17
Sil-M (front)	0.33	0.12
Sil-M (middle)	0.28	0.11
Sil-M (rear)	0.29	0.10

imately 15 % of the material, indicating a significant amount of immobilized catalyst. Additionally, the data reveal the stability of the immobilized catalyst up to temperatures around 250 °C, which makes reaction conditions at elevated temperatures feasible.

To quantify the catalyst loading of the functionalized silica materials, elemental analysis was employed, and the amount of catalyst was calculated based on the nitrogen content of the sample. Table 1 lists the amine loadings after the first functionalization step as well as the final catalyst loading of the different materials. For the norbornene intermediate, no loading could be determined through this method, as the number of nitrogen atoms remains unchanged upon reaction.

With the particles possessing larger mesopores of 30 nm, a comparatively low catalyst loading of 0.09 mmol g^{-1} was obtained. By decreasing the pore size and thus increasing the surface area that can be modified, the catalyst loading increased almost twofold to 0.17 mmol g^{-1} for the Sil-P10 particles. For the silica monolith, the results confirm a slight gradient of catalyst distribution, as already suggested by physisorption. Still, the monolith carries a significant amount of catalyst in all parts.

In none of the support materials the initially high amine loadings were completely transformed into the catalyst motif. Indeed, the presence of unreacted NH_2 groups was confirmed by Kaiser tests with the final material (see SI *Figure S3*). The limiting step of the functionalization therefore appears to be the coupling reaction with the norbornene carboxylic acid, which even after repeating did not result in a complete conversion. Capping of residual amino groups, e.g. with acetic anhydride, was not performed in order to prevent further crowding of the silica surface which might interfere with the subsequent functionalization step. Furthermore, since the residual amine groups were obviously not accessible during the repetitive norbornene coupling reaction, it is expected that their influence on the catalysis in the final material, neighboring the sterically demanding catalyst motif, can be neglected.

Organocatalysis with the silica supported catalyst

As a model reaction, the enamine-catalyzed addition of β-nitrostyrene and *n*-butanal was chosen (Scheme 1).

Prior to the investigation of the set of supported catalysts, a number of tripeptide derivatives (1.00 mol-%) were tested in a

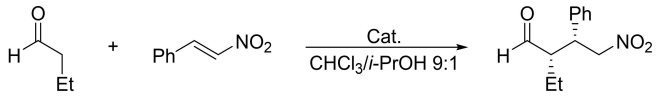

Scheme 1. Model reaction of *n*-butanal and ß-nitrostyrene yielding the corresponding γ-nitroaldehyde.

homogeneous reaction (Table 2). Applying similar reaction conditions as reported previously, the results can be compared.[4,7] The Tz-Catalyst shows, within the error of the experiment, similar conversions, and reaches related *syn/anti*-ratios as well as enantioselectivities comparable to the unmodified D-Pro-Pro-Glu (see SI *Figure S8* for UHPLC kinetics), its enantiomer Pro-D-Pro-D-Glu or the racemic mixture described by Wennemers and coworkers. Thus, neither the 1,6-diaminohexyl-linker nor the Tz moiety required for the IEDDA ligation jeopardize the catalyst performance. Using no catalyst (Control) or Tz-Pro it is affirmed that the tripeptide is required for both the high yields and the enantioselectivity.

Table 2. Results of the reactions of *n*-butanal (1.50 eq.) and ß-nitrostyrene (1.00 eq.) using different homogeneous derivatives of the catalyst (RT, 16 h).

Compound	Conversion/%[a]	*syn/anti*[a]	*ee*/%[b]
Control	0	–	–
d-Pro-Pro-Glu	97	97:3	96
Pro-d-Pro-d-Glu	97	94:6	95
Rac. mixture	97	97:3	0
Tz-Catalyst	98	94:6	95
Tz-Pro	67	89:11	31

[a] Determined by UHPLC; [b] Determined by chiral stationary phase HPLC analysis.

Table 3. Results of the reactions of *n*-butanal (3.00 eq.) and ß-nitrostyrene (1.00 eq.) using functionalized silica particles in a batch setup. [Conditions]: $CHCl_3$/*i*-PrOH (9:1), RT, 16 h.

Entry[a]	Catalyst	Conversion/%[d]	*syn/anti*[d]	*ee*/%[e]
–OH	Sil-P10/30	0	–	–
–NH2	Sil-P10/30	0	–	–
A1	Sil-P30	7	99:1	80
B1	Sil-P30	99	93:7	86
C1[b]	Sil-P30	99	91:9	84
D1	Sil-P10	69	96:4	87
Recycling				
B2	Sil-P30	4	93:7	69
B3[c]	Sil-P30	7	91:9	69
C2[b]	Sil-P30	47	91:9	79
C3[b]	Sil-P30	23	91:9	81
D2	Sil-P10	62	96:4	–
D3	Sil-P10	38	95:5	80

[a] Entry A with ß-nitrostyrene (0.33 mol L^{-1}) and entries B–D with ß-nitrostyrene (0.59 mol L^{-1}); [b] Entries C1-3 at 50 °C; [c] five wash steps with NEt_3 (1% in DCM); [d] Determined by UHPLC; [e] Determined by chiral stationary phase HPLC analysis.

Based on these results, the catalyst-loaded silica phases were investigated initially in batch reactions (3.00 eq. of *n*-butanal, 1.00 eq. of β-nitrostyrene) to evaluate the catalytic activity and selectivity. A control test in the presence of unfunctionalized Sil-P10/30-OH particles did not yield any reaction products. Additionally, to investigate the effect of unreacted amine groups on the catalysis, the Sil-P10/30-NH_2 materials were used under the same reaction conditions as the catalyst material, and similar to other control tests no formation of any products could be observed. Using 1.00 mol% of the Sil-P10/30-Cat particles the conversion of β-nitrostyrene to the products was determined after 16 h using UHPLC (Table 3). Starting with the particles with a mesopore size of 30 nm (loading: 0.09 mmol g^{-1}) and a concentration of 0.33 mol L^{-1} for nitrostyrene, a yield of only 7% could be reached after 16 hours (Table 3, Entry A1). Increasing to a concentration of 0.59 mol L^{-1} for Sil-P30-Cat material resulted in a yield of 99% (Table 3, Entry B1), presumably because of an increased contact frequency of the reactant with the catalytic sites. Using a higher temperature of 50 °C in the catalysis, the yield and the selectivities remain unaffected, while Wennemers *et al.* have shown that this has a negative effect on the *syn/anti* selectivity and the enantiomeric excess (Table 3, Entry C1). With the particles possessing smaller mesopores (loading: 0.17 mmol g^{-1}), a yield of 69% could initially be obtained, the lower conversion presumably being related to the smaller pore size and the accompanying diffusion limitations (Table 3, Entry D1).

Beyond that, the materials were washed afterwards and used in recycling experiments for two more rounds (Table 3, Entries B2-D3). For the Sil-P30 particles the yield dropped tremendously to 4% when recycled, which also could not be raised again by reactivation of the material by a base treatment with NEt_3. The enantiomeric excesses also decreased to 69%. The recycling experiments with the 50 °C reactions did not result in such a sharp drop in conversions, while the *syn/anti* ratios remained constant and the enantiomeric excesses stayed high. The experiments with the Sil-P10 particles showed better results in recycling. Generally, the selectivities were in the same range regardless of the particle sizes during all reactions. Besides of a small possible loss of material through the recycling steps, an assumed deactivation of the catalyst through protonation after the first runs then led to a further drop in yields for the subsequent entries, which a wash step with NEt_3 (Entry B3) could not reverse.[7]

In addition to that, it was tested for Sil-P10-Cat whether the conversion of β-nitrostyrene to the product mixtures could be completed by increasing the reaction time. UHPLC kinetics showed that all reactant was consumed after 72 h (see SI *Figure S8*).

After having confirmed the catalytic activity in batch, the next step was the implementation in a continuous flow setup. For that reason, both types of particles were packed into stainless steel columns (50×4 mm) to be used as packed bed reactors that can be connected to an HPLC pump. Similarly, the

silica monoliths were cladded in polyether ether ketone (PEEK) to be used as continuous flow reactors as well. The reaction was followed with chiral stationary phase HPLC chromatography, where after a specific time an aliquot of the solution leaving the reactor was investigated (see SI *Figure S9*).

When using a packed bed reactor with Sil-P30-Cat, only low yields up to 24% were achieved (Table 4, entries 1–3). However, when assessing the performance of a catalyst system, an important parameter beyond the product conversion is the turnover frequency (TOF), which considers the amount of catalyst as well. The TOF values were calculated according to equation 1, where, in case of the flow reactions, the flow rate F is used and the amount of catalyst $n_{catalyst}$ is calculated based on the amount of material inside the reactor and its catalyst loading.

Table 4. Flow catalysis of the reaction between *n*-butanal and ß-nitrostyrene using packed bed and monolithic silica reactors.[a]

Entry	Catalyst	Time/h	Conversion[b]/%	*ee*[b]/%	TOF/h^{-1}
1	Sil-P30	1	22	[c]	15
		2	18	[c]	12
		3	18	[c]	12
2	Sil-P30	1	14	[c]	10
		2	15	[c]	10
		3	13	[c]	9
		24	4	[c]	3
3	Sil-P30	1	9	[c]	6
		2	24	86	17
		3	17	83	12
		4	9	83	6
4	Sil-P10	1	68	86	24
		2	95	86	34
		3	58	86	21
5	Sil-P10	1	60	88	21
		2	58	87	21
		3	52	87	19
		24	23	86	8
6[d]	Sil-P10	1	39	83	14
		2	36	83	13
		3	35	82	13
		4	28	82	10
		5	26	80	9
7[e]	Sil-P10	1	100	79	2
8	Sil-M	1	20	86	38
		2	18	88	34
		3	17	87	33

Different entries mark separate experiments, reusing the same reactor (unless otherwise noted), but with a wash step before and after each use. [a] ß-nitrostyrene (0.3 mol L^{-1} in $CHCl_3$/*i*-PrOH (9:1)), *n*-butanal (6.00 eq.), room temperature; [b] determined by chiral stationary phase HPLC analysis; [c] not determined; [d] after treatment with NEt_3 (1.00% in DCM); [e] flow interrupted and solution kept inside the reactor for 1 h.

$$TOF = \frac{n_{product}}{n_{catalyst} \cdot t_{reaction}} = \frac{c_{product} \cdot F}{n_{catalyst}} \quad (1)$$

With Sil-P30-Cat, TOF values up to 17 h^{-1} were reached at room temperature, which is comparable to results of other functionalized silica materials used in heterogeneous organocatalysis.[21,22] Therefore, the material does show a significant catalytical activity and the relatively low reaction yields rather seem to be caused by the small amount of material that is used in a reactor of that dimension. Indeed, using Sil-P10-Cat, conversions up to 68% were possible (entries 4 and 5), with slightly higher TOF values of up to 24 h^{-1}. Presumably, this improvement is due to the increased amount of catalyst inside the reactor, as the catalyst loading for Sil-P10-Cat is higher, while the amount of silica used for packing stays mostly unchanged. Similar to before, the reaction yield decreases over time. Beside catalyst deactivation, another reason could be a diffusion limitation that hinders the formed product to leave the smaller mesopores and thus occupying the active sites of the silica surface. Indeed, prolonged washing in between reaction cycles did lead to increased yields for subsequent reactions, although the downward trend could not be prevented entirely upon further usage. Also, physisorption experiments of the material after usage confirm that the mesopore system remains intact, suggesting the catalyst sites are still accessible even after multiple cycles (*Figures S5* and *S6*). Likewise, the DRIFT spectrum of the used material does not show any additional bands, making significant chemical changes to the catalyst unlikely (*Figure S7*). In an attempt to reactivate the catalyst by deprotonation, the reactor was also washed with a solution of NEt_3 (1% in DCM), which resulted in only slightly higher conversions for the following cycle (entry 6). In a different experiment (entry 7), the reaction solution was pumped into the reactor before the flow was interrupted and the solution kept inside for 1 hour, to increase the contact time between reagent and catalyst. The solution exiting the reactor was then analyzed analogously as before and a quantitative conversion of the substrate could be observed, confirming that there is no inherent limitation of the catalyst preventing higher conversions upon immobilization to the silica surface. Instead, the flow process itself must be optimized in a way to guarantee sufficient contact times as well as intermittent wash steps. Finally, the functionalized silica monolith was also used for flow catalysis, achieving yields up to 20% (entry 8). Because of the low amount of material in only one silica monolith and hence a low amount of catalyst, the TOF values are exceptionally high despite the low conversion numbers. An improvement of the overall performance could thus be achieved by a scaling up procedure, which is easily implemented by numbering up through connecting multiple monoliths.

While the particles with larger mesopores yielded slightly better results in the batch experiments, in the flow setup, the Sil-P10 particles outperform the Sil-P30 particles noticeably, partly due to the abovementioned increase in catalyst loading. However, both Sil-P10 and especially the silica monolith Sil-M also show an increase in the TOF values, which take this

difference in catalyst loading into account. Concludingly, possible diffusion limitations caused by a lower average mesopore size seem to be negligible in the flow reactions. In case of the silica monolith, the more important aspect seems to be pore accessibility, which governs the ability of the substrate molecules to reach the active catalyst sites in the pore network. Especially for the monolithic silica which has a higher porosity and a smaller skeleton thickness, this results in a much higher productivity compared to the other materials, even though the yield is limited by the low catalyst amount in a single monolith.

With all three materials, high enantioselectivities of up to 87% were achieved, which is however still a decrease compared to the homogeneous reactions. A possible explanation could be the smaller energy difference between both diastereomeric transition states as well as spatial confinement effects that hinder the formation of the transition state in the correct conformation. However, the enantioselectivity appears to be independent of the mesopore size, as no difference can be observed between the different materials. Considering the size of the substrate compared to the pore size which ranges up to 30 nm, a dramatic confinement effect is also unlikely. Another reason therefore could be the silica surface itself. Possibly, the slightly acidic silanol groups which remain on the surface might interfere in formation of the transition state or alter the orientation of the catalyst in a way that impedes the formation of a preferred enantiomer.

Conclusions

Within this study, the peptide-based organocatalyst D-Pro-Pro-Glu was immobilized on two different silica materials for continuous flow catalysis. The catalyst was synthesized by solid phase peptide synthesis and then modified with a tetrazine linker for the functionalization by inverse electron-demand Diels-Alder reaction (IEDDA) with the norbornene functionality on the modified silica surface. Through homogeneous test reactions in the conjugate addition between ß-nitrostyrene and *n*-butanal it could be shown that the modifications to the catalyst did not lead to any decrease in activity compared to the catalyst as prepared previously in literature. The immobilization of the organocatalyst was confirmed by argon physisorption, DRIFT and TGA-MS and quantified by elemental analysis, yielding loadings up to 0.2 mmol g^{-1}. All materials proved to successfully catalyze the enantioselective addition reaction between *n*-butanal and ß-nitrostyrene. Especially for the particles with 30 nm mesopores, high catalyst loadings (in batch) or long residence times (in flow) were needed to achieve satisfying yields. The materials with smaller mesopores performed notably better, which was explained by the increased catalyst loading on the material but also by a more accessible pore network in the case of the silica monoliths. The enantiomeric excess of the product in the heterogeneous catalysis was found to be slightly lower than in the homogeneous reaction, which suggests the polar silica surface interferes in the formation of a preferred conformation during the transition state. Further improvements could be achieved by endcapping of the remaining silanol groups with small inert groups, for example through reaction with hexamethyldisilazane. Lastly, especially the monolithic reactor reached very high turnover frequencies, indicating the potential of the material for future catalytic applications in a scaled-up system.

Experimental Section

Materials

LiCrospher Si100 (Merck) and PerfectSil 300 silica particles were purchased from mz-Analysentechnik GmbH.

The chemicals (3-aminopropyl)trimethoxysilane (97%, APTMS), ß-nitrostyrene (99%), *n*-butanal (≥ 99.5%), urea (99.5%), sodium nitrite (>97%, $NaNO_2$), 4-(dimethylamino)pyridine (99%, DMAP), hexamethylenediamine (98%), triethylsilane (99%), 4-methylmorpholine (≥ 99.5%, NMM) and triethylamine (99.5%, NEt_3) were purchased from Sigma-Aldrich (Merck). *N*-(3-dimethylaminopropyl)-*N'*-ethylcarbodiimide hydrochloride (99%, EDC) and PyBOP (≥ 98.5%) were purchased from Carl Roth, acetic acid (99.5%), NaCl (99%) and $MgSO_4$ (99%) from Grüssing GmbH. 4-Cyanobenzoic acid (>98%), hydrazine monohydrate (65% in H_2O, >98%), 5-norbornene-2-carboxylic acid (*endo*-/*exo*-mixture, 98%), *N*-hydroxysuccinimide (>98%) and Boc-D-Pro-OH (peptide grade) were purchased from TCI. Zinc triflate (98%) was purchased from abcr, tetramethyl orthosilicate (99%) from Thermo Fisher Scientific, polyethylene glycol 10.000 from Fluka and hexafluoroisoproyl alcohol (99%, HFIP) from Carbolution. DIPEA (peptide grade), piperidine (peptide grade), TFA (peptide grade), 2-chlorotrityl chloride (CTC) resin (loading: 1.6 mmol g^{-1}), Fmoc-Rink Amid AM resin (loading: 0.74 mmol g^{-1}), as well as the amino acids (peptide grade) Fmoc-Pro-OH, Fmoc-D-Pro-OH, Fmoc-Glu(*t*Bu)-OH and Fmoc-D-Glu(*t*Bu)-OH were purchased from Iris Biotech. Ethylamine (2 M in THF) was purchased from Alfa Aesar, NH_4Cl (99.5%) and HCl (37%) from Acros Organics. Solvents were purchased from VWR as HPLC or peptide grade or distilled before use.

Essential Experimental Procedures/Data

Syntheses of low molecular tetrazines and norbornenes

Synthesis of Tz-COOH[19,27] 200 mg (1.36 mmol) of 4-cyanobezoic acid were solved with 247 mg (0.68 mmol) of zinc triflate in 5.20 mL (69.0 mmol) hydrazine monohydrate and 0.70 mL (13.6 mmol) acetonitrile under argon atmosphere and stirred under reflux at 60 °C for 24 h. The suspension was cooled down and 1.88 g (27.2 mmol) of $NaNO_2$, dissolved in 5 mL H_2O, was added. The suspension was acidified with 120 mL HCl (1 M) to pH = 1. The pink suspension was extracted three times with ethyl acetate and the combined organic phases were dried over $MgSO_4$, filtered, and concentrated under reduced pressure. Column chromatography with DCM/MeOH/acetic acid (100:1:0.1) provides 222 mg (1.03 mmol) of the pink solid **Tz-COOH** in a yield of 76%. **^{1}H-NMR (500 MHz, DMSO-d_6)**: δ (ppm) = 13.34 (s, 1H, COO*H*), 8.57 (m, 2H, Ar-*H*), 8.21 (m, 2H, Ar-*H*), 3.02 (s, 3H, CH_3); **ESI-QMS**: $[M+H]^+$ calculated for $C_{10}H_8N_4O_2$: *m/z* = 217.06; found: *m/z* = 217.25.

Synthesis of Tz-NHS ester[19,28] 500 mg (2.31 mmol) of Tz-COOH were mixed with 537 mg (2.80 mmol) of EDC x HCl, 322 mg (2.80 mmol) of *N*-hydroxysuccinimide and 11 mg (0.09 mmol) of DMAP in 40 mL THF and then stirred at room temperature for 27 h. After that, the suspension was diluted with 100 mL H_2O and extracted eight times with 100 mL ethyl acetate each. The organic

phase was washed two times with 250 mL saturated NaCl solution, dried over $MgSO_4$ and concentrated under reduced pressure. The residue was purified with column chromatography with DCM. 423 mg (1.35 mmol) of **Tz-NHS ester** was obtained as a pink crystalline solid in a yield of 58%. **^{1}H-NMR (500 MHz, $CDCl_3$)**: δ (ppm) = 8.76 (m, 2H, Ar-*H*), 8.37 (m, 2H, Ar-*H*), 3.15 (s, 3H, CH_3), 2.95 (s, 4H, CH_2); **ESI-QMS**: $[M+H]^+$ calculated for $C_{14}H_{11}N_5O_4$: *m/z* = 314.08; found: *m/z* = 314.16.

Syntheis of Tz-CONHEt[28] 310 mg (1.00 mmol) of **Tz-NHS ester** was dissolved in 10 mL DCM. After adding 700 µL (4.00 mmol) of DIPEA, 1.50 mL (3.00 mmol) of ethylamine (2 M in THF) was added dropwise and the solution was stirred at room temperature for 3 h. The solvent was removed under reduced pressure and the residue was dissolved in 50 mL DCM, washed three times with 50 mL H_2O and two times with saturated NaCl solution. The organic phase was dried over $MgSO_4$ and the solvent was removed under reduced pressure. The residue was purified by column chromatography with MeOH/DCM (1 : 4) to get 239 mg (0.98 mmol) of the pink, crystalline **Tz-CONHEt** in a yield of 98%. **^{1}H-NMR (500 MHz, $CDCl_3$)**: δ (ppm) = 8.67 (m, 2H, Ar-*H*), 7.98 (m, 2H, Ar-*H*), 6.23 (s, 1H, N*H*), 3.56 (m, 2H, CH_2), 3.12 (s, 3H, CH_3), 1.30 (t, *J* = 7.1 Hz, 3H, CH_2CH_3); **ESI-QMS**: $[M+H]^+$ calculated for $C_{12}H_{13}N_5O$: *m/z* = 244.12; found: *m/z* = 244.22.

Synthesis of Nb-NHS ester[34] 402 mg (2.91 mmol) of *endo*-/*exo*-5-norbornene-2-carboxylic acid was dissolved in 15 mL DCM. 696 mg (3.63 mmol) of EDCl and 418 mg (3.63 mmol) of *N*-hydroxysuccinimide were added. The clear mixture was stirred at room temperature for 24 h, before the solvent was removed under reduced pressure. The residue was dissolved in 200 mL ethyl acetate, washed two times with 100 mL saturated NH_4Cl solution, two times with 100 mL saturated $NaHCO_3$ solution and two times with 100 mL saturated NaCl solution. The organic phase was dried with $MgSO_4$ and concentrated under reduced pressure. 467 mg (1.99 mmol) of **Nb-NHS ester** (*endo*-/*exo*-mixture) was obtained as a white crystalline solid in a yield of 96%. **^{1}H-NMR (500 MHz, $CDCl_3$)**: δ (ppm) = 6.24 (m, 1H, C=C*H*), 6.13 (m, 1H, C=C*H*), 3.25 (m, 1H, C*H*), 2.99 (m, 1H, C*H*), 2.80 (m, 4H, CH_2), 2.51 (m, 1H, O=CC*H*), 2.02 (m, 1H, C*H*), 1.51 (m, 2H, CH_2), 1.35 (d, *J* = 8.3 Hz, 1H, C*H*); **ESI-QMS**: $[M+H]^+$ calculated for $C_{12}H_{13}NO_4$: *m/z* = 236.08; found: *m/z* = 236.18, 236.31.

Synthesis of Nb-CONHEt[35] 299 mg (1.27 mmol) of **Nb-NHS ester** was dissolved in 6 mL DCM. 648 µL (3.81 mmol) of DIPEA and 1.3 mL (2.54 mmol) of ethylamine (2 M in THF) were added dropwise. The white suspension was then stirred at room temperature for 2 h. The mixture was filtered and the residue was dried under reduced pressure. After column chromatography with ethyl acetate/*n*-hexane (4 : 1), 162 mg (0.98 mmol) of the white, crystalline **Nb-CONHEt** was obtained as the *endo*-/*exo*-mixture in a yield of 41%. **^{1}H-NMR (500 MHz, $CDCl_3$)**: δ (ppm) = 6.27 (m, 1H, C=C*H*), 5.98 (m, 1H, C=C*H*), 5.63 (s, 1H, N*H*), 3.21 (s, 1H, C*H*), 3.04 (m, 1H, C*H*), 2.94 (s, 1H, O=CC*H*), 1.99 (m, 1H, C*H*), 1.47 (d, *J* = 7.7 Hz, 1H, C*H*), 1.40 (m, 2H, NCH_2), 1.34 (m, 1H, C*H*), 1.25 (m, 1H, C*H*), 1.12 (m, 3H, CH_3); **ESI-QMS**: $[M+H]^+$ calculated for $C_{10}H_{15}NO$: *m/z* = 166.12; found: *m/z* = 166.26, 166.29.

Syntheses of peptides[24,26]

Preloading of the 2-chlorotrityl chloride (CTC) resin 1.0 g (1.6 mmol) of 2-chlorotrityl chloride resin (loading: 1.60 mmol/g) were put in a syringe reactor and swollen in 7.5 mL DCM. After removing of the solvent, 2.21 g (19.0 mmol) of hexamethylenediamine, dissolved in 7.5 mL DCM, were added to the resin and reacted at room temperature for 22 h. The solvent was removed and the resin was capped with a solution of 8.5 mL DCM, 1.0 mL MeOH and 500 µL DIPEA at room temperature for 30 min. The resin was washed three times with DCM, DMF and again DCM and dried under reduced pressure. The loading of 0.70 mmol/g for the preloaded CTC resin was determined with an Fmoc-test using Fmoc-Ala-OH (see SI).[36]

Synthesis of Tz-Pro 250 mg (0.175 mmol) of the preloaded CTC resin (loading: 0.70 mmol/g) were put in a syringe reactor and swollen in 5 mL DMF. After removing the DMF, a solution of 113 mg (0.525 mmol) of Boc-D-Pro, 273 mg (0.525 mmol) of PyBOP and 119 µL (0.70 mmol) of DIPEA in 2 mL DMF was added to the resin and reacted at room temperature for 45 min. After repetition of the reaction, the resin was washed three times with DMF, DCM, DMF, then ten times with DCM, before the peptide was cleaved off of the resin with 5 mL HFIP (20% in DCM) two times at room temperature for 30 min and concentrated under reduced pressure. Analytics of intermediate (brown oil): **ESI-QMS**: $[M+H]^+$ calculated for $C_{16}H_{31}N_3O_3$: *m/z* = 412.50; found: *m/z* = 412.50.

57 mg (0.18 mmol) of the Boc-protected peptide was reacted with 56 mg (0.18 mmol) of **Tz-NHS ester** and 61 µL (0.36 mmol) of DIPEA in 3 mL DCM at room temperature for 2 h. After that, 750 µL TFA were added and reacted for another 4 h. After removing the solvent in argon stream, the peptide was precipitated three times in cold Et_2O, suspended in H_2O and dried with lyophilization. The Tz-Pro (62.9 mg, 0.15 mmol) was obtained as a pink solid in a yield of 85%. **^{1}H-NMR (500 MHz, DMSO-d_6)**: δ (ppm) = 9.51 (s, 1H, N*H*), 8.72 (t, *J* = 5.6 Hz, 1H, N*H*), 8.53 (d, *J* = 8.1 Hz, 2H, Ar-*H*), 8.08 (d, *J* = 8.1 Hz, 2H, Ar-*H*), 4.12 Hz (t, *J* = 7.8 Hz, 1H, N*H*), 3.29 (m, 2H, CH_2), 3.17 (m, 5H, CH_2), 3.01 (s, 3H, CH_3), 2.27 (m, 1H, CH_2), 1.88 (m, 2H, CH_2), 1.80 (m, 1H, CH_2), 1.54 (m, 2H, CH_2), 1.45 (m, 2H, CH_2), 1.32 (m, 4H, CH_2); **ESI-QMS**: $[M+H]^+$ calculated for $C_{21}H_{29}N_7O_2$: *m/z* = 411.24; found: *m/z* = 412.50.

Synthesis of Tz-Catalyst 1.00 g (0.70 mmol) of the preloaded CTC resin (0.70 mmol/g) were put in a round bottom flask and swollen in 20 mL DMF. After removing the DMF, the resin was shaken twice each with a solution of 1.09 g (2.10 mmol) PyBOP, 536 µL (3.15 mmol) of DIPEA and one amino acid (893 mg (2.10 mmol) of Fmoc-Glu(*t*Bu)-OH, 708 mg (2.10 mmol) of Fmoc-Pro-OH and 452 mg (2.10 mmol) of Boc-D-Pro-OH) in 20 mL DMF at room temperature for 45 min. When changing to a new amino acid, the resin was deprotected twice with 20 mL piperidine (20% in DMF) and washed with DMF, DCM and again DMF. After the last coupling reaction, the resin was washed three times with DMF, DCM, DMF, then ten times with DCM, before the peptide was cleaved off of the resin with 20 mL HFIP (20% in DCM) four times at room temperature for 30 min and concentrated under reduced pressure. Analytics of intermediate (brown oil): **ESI-QMS**: $[M+H]^+$ calculated for $C_{30}H_{53}N_5O_7$: *m/z* = 596.39; found: *m/z* = 596.36.

357 mg (0.60 mmol) of the Boc-protected peptide was reacted with 226 mg (0.72 mmol) of **Tz-NHS ester** and 255 µL (1.50 mmol) of DIPEA in 40 mL DCM at room temperature for 3 h. After that, 4 mL TFA were added and reacted for another 4 h. After removing the solvent in argon stream, the peptide was precipitated three times in cold Et_2O, suspended in H_2O and dried with lyophilization. The Tz-Catalyst (287 mg, 0.45 mmol) was obtained as a pink solid in a yield of 75%. **^{1}H-NMR (500 MHz, DMSO-d_6)**: δ (ppm) = 8.70 (t, *J* = 5.7 Hz, 1H, N*H*), 8.54 (d, *J* = 8.4 Hz, 2H, Ar-*H*), 8.26 (d, *J* = 7.8 Hz, 1H, N*H*), 8.09 (d, *J* = 8.4 Hz, 2H, Ar-*H*), 7.78 (t, *J* = 5.5 Hz, 1H, N*H*), 4.49 (t, *J* = 7.6 Hz, 1H, N*H*), 4.38 (dd, *J* = 8.7 Hz, *J* = 2.8 Hz, 1H, C*H*), 4.16 (m, 1H, C*H*), 3.67 (m, 1H, C*H*), 3.29 (q, *J* = 6.5 Hz, 1H, CH_2), 3.13 (m, 1H, CH_2), 3.02 (s, 3H, CH_3), 2.38 (m, 1H, CH_2), 2.21 (m, 1H, CH_2), 2.08 (m, 1H, CH_2), 1.87 (m, 7H, CH_2), 1.74 (m, 1H, CH_2), 1.54 (m, 2H, CH_2), 1.41 (m, 2H, CH_2), 1.31 (m, 4H, CH_2), 1.25 (d, *J* = 6.5 Hz, 1H, CH_2); **ESI-QMS**: $[M+H]^+$ calculated for $C_{31}H_{43}N_9O_6$: *m/z* = 638.33; found: *m/z* = 638.29.

Synthesis of H-D-Pro-Pro-Glu-NH_2 [4] 338 mg (0.25 mmol NH_2) of Fmoc-Rink Amid Am resin (loading: 0.74 mmol/g) was filled in a syringe reactor and swollen in 5.0 mL NMP. After Fmoc deprotection with 2.0 mL piperidine (20% in NMP), each amino acid (425 mg (1.00 mmol) of Fmoc-Glu(*t*Bu)-OH, 337 mg (1.00 mmol) of Fmoc-Pro-OH and 337 mg (1.00 mmol) of Fmoc-D-Pro-OH) was dissolved in 5.0 mL NMP with 520 mg (1.00 mmol) PyBOP and 0.26 mL (1.50 mmol) DIPEA and reacted twice for 45 min at room temperature with the deprotected resin each. Before switching to the next amino acid, the Fmoc groups were cleaved off with 2.0 mL piperidine (20% in NMP). After the final Fmoc deprotection, the peptide was cleaved off from the resin with a solution of 9.5 mL TFA, 0.45 mL triethylsilane and 50 μL H_2O. After precipitation in cold Et_2O, dissolving in H_2O and lyophilization 68 mg (0.20 mmol) of the white tripeptide was obtained in a yield of 80%. **^{1}H-NMR (500 MHz, D_2O)**: δ (ppm) = 4.60 (dd, J = 7.2 Hz, 9.0 Hz, 1H), 4.42 (dd, J = 4.1 Hz, 9.6 Hz, 1H), 4.30 (dd, J = 5.3 Hz, 9.3 Hz, 1H), 3.69 (m, 1H), 3.57 (m, 1H), 3.38 (m, 2H), 2.51 (m, 1H), 2.45 (m, 3H), 2.28 (m, 1H), 2.03 (m, 8H); **ESI-QMS**: $[M+H]^+$ calculated for $C_{15}H_{24}N_4O_5$: m/z = 341.17; found: m/z = 341.32.

Synthesis of H-Pro-D-Pro-D-Glu-NH_2 [4] Same procedure as for **H-D-Pro-Pro-Glu-NH_2**, but with 425 mg (1.00 mmol) of Fmoc-D-Glu(*t*Bu)-OH, 337 mg (1.00 mmol) of Fmoc-D-Pro-OH and 337 mg (1.00 mmol) of Fmoc-Pro-OH). 62 mg (0.18 mmol) of the white tripeptide was obtained in a yield of 72%. **^{1}H-NMR (500 MHz, D_2O)**: δ (ppm) = 4.60 (dd, J = 7.1 Hz, 9.0 Hz, 1H), 4.43 (dd, J = 4.1 Hz, 9.6 Hz, 1H), 4.30 (dd, J = 5.3 Hz, 9.4 Hz, 1H), 3.69 (m, 1H), 3.57 (m, 1H), 3.51 (q, J = 7.0 Hz, 0.5H), 2.52 (m, 1H), 2.45 (m, 2H), 2.28 (m, 1H), 2.03 (m, 8H), 1.13 (t, J = 7.0 Hz, 0.5H); **ESI-QMS**: $[M+H]^+$ calculated for $C_{15}H_{24}N_4O_5$: m/z = 341.17; found: m/z = 341.19.

Preparation of catalyst materials

Functionalization of silica particles with APTMS 0.500 g of silica particles were dried under vacuum at 80 °C overnight and suspended in 20 ml toluene. Then, 166 μL (0.95 mmol) of 3-(aminopropyl) trimethoxy silane and 50.0 μL of water were added. The suspension was stirred for 24 h at 80 °C and afterwards the solvent was removed via centrifugation. The particles were washed with toluene, DCM, MeOH and MeOH/H_2O (1 : 1) and then dried under vacuum at 40 °C overnight.

Functionalization of silica particles with norbornene 873.9 mg of amine-functionalized silica particles were suspended in 80 mL DCM. After adding 1.71 mL (13.98 mmol) of 5-norbornene-2-carboxylic acid, 536.5 mg (2.80 mmol) of EDC x HCl, 282.9 mg (2.80 mmol) of DMAP and 390 μL (2.80 mmol) of NEt_3, the suspension was shaken for five days at room temperature on a laboratory shaker. After that, the solvent was removed via centrifugation and the particles were washed with DCM, MeOH and MeOH/H_2O (1 : 1) and then dried under vacuum at 40 °C overnight.

Functionalization of silica particles with Tz-Catalyst 600 mg of norbornene-functionalized silica particles together with 2.091 g (3.35 mmol) of Tz-Catalyst were suspended in 100 mL DMF and shaken (not stirred, to prevent damaging the particles) at 80 °C in a water bath overnight. After removing the solvent via centrifugation, the now yellow particles were washed with DMF, DCM, MeOH and MeOH/H_2O (1 : 1), and then dried under vacuum at 40 °C overnight.

Synthesis of silica monoliths 1.20 g polyethylene glycol 10.000 and 0.90 g urea were dissolved in 10 mL acetic acid (0.01 M) and stirred at room temperature for 35 min. After cooling in an ice bath, 5.6 mL tetramethoxysilane were added and the solution was stirred for another 20 min at 0 °C. After warming to room temperature again, the solution was transferred to stainless steel tubes and aged at 22.5 °C in a water bath for 22 h. The obtained silica monoliths were then placed in a urea solution (9 g urea in 100 mL 0.01 M acetic acid) and placed in a furnace for hydrothermal treatment (method A: heating to 95 °C over 12 h and holding the temperature for another 15 h, method B*:* heating to 110 °C over 14 h and holding the temperature for another 15 h). The silica monoliths were then placed in MeOH and shaken on a laboratory shaker for five day during which the MeOH was replaced three times. Subsequently, the monoliths were placed in a furnace for calcination (heating to 330 °C over 10 h and holding the temperature for another 15 h.). For the cladding process, the monoliths were put into a PEEK tube surrounded by a PTFE shrink tube and heated to 362 °C.

Characterization methods

Argon physisorption experiments were performed using an "Autosorb iQ" instrument by Quantachrome Instruments at a temperature of 87 K using a CryoSync cryostat. Pore size distributions were calculated using an NLDFT kernel (Ar at 87 K, zeolites/silica, cylindr. pores, adsorption branch) provided by the Quantochrome software ASiQwin.

Nitrogen physisorption experiments were performed using a "Quadrasorb evo" instrument by Quantachrome Instruments at a temperature of 77 K. Pore size distributions were calculated using an NLDFT kernel (N_2 at 77 K, silica, cylindr. pores, adsorption branch).

Elemental analysis was performed using a CHN-analyzer Flash EA-1112 by Thermo Scientific.

For scanning electron microscopy, the sample was sputter coated with platinum and measured with a Zeiss Merlin (acceleration voltage of 2.00 kV, current of 113 pA).

Ultra-performance liquid chromatography with electron spray ionization mass spectrometry (UHPLC-ESI-QMS) was performed with an ACUIDITY-UPLC® H-Class CM Core System of Waters GmbH. Detection was done with an ACUIDITY-UPLC® photo diode array (PDA)-detector and an ACUIDITY-UPLC® QDa mass detector (ESI-ionization).

UV-Vis measurement was performed using a UV-2501PC UV-Vis-spectro-meter by Shimadzu Deutschland GmbH.

HPLC measurements were performed using a Dionex P680 pump equipped with a Degasys DG2410 Degasser and a Dionex UVD170 U detector for separation. Chiralpak IC and Eurospher II CN columns were used, with a solvent mixture of 85% n-hexane and 15% methyl *tert*-butyl ether and a flowrate of 1.2 mL min^{-1}.

UV-Vis Kinetics of IEEDA reactions[30,31]

Homogeneous IEDDA

In each case, one Tz (1.00 eq., 20 mg/mL) was reacted with one Nb (1.60 eq.) in DMF at 80 °C. The solutions were examined using UV-Vis spectroscopy by diluting 25 μL of the reaction solutions with 975 μL DMF at specific times and measuring them in glass cuvettes, until the absorption maxima at λ_{max} = 538 nm remained constant.

Heterogeneous IEDDA

Tz-NEt (1.00 eq, 3.63 mg/mL) was added to a suspension of Sil-P10-Nb (1.00 eq) and Sil-P30-Nb (1.00 eq.) in DMF and reacted at 80 °C. The solutions were examined using UV-Vis spectroscopy by diluting 20 μL of the centrifugated reaction mixtures with 480 μL DMF at

specific times and measuring them in glass cuvettes, until the absorption maxima at $\lambda_{max} = 538$ nm remained constant.

Catalytic tests

Homogeneous catalysis

1.00 mol% of H-D-Pro-Pro-Glu-NH_2, H-Pro-D-Pro-D-Glu-NH_2, a racemic mixture of both, Tz-Pro and Tz-Catalyst was reacted each with 297 μL (3.29 mmol) of *n*-butanal, 328 mg (2.20 mmol) of β-nitrostyrene and 2.4 μL (1.00 mol-%) of NMMin 5 mL $CHCl_3$/*i*-PrOH (9:1) at room temperature for 16 h. After this time, the solutions were examined with UHPLC-ESI-QMS for the reaction conversions and the *syn*/*anti* ratios of the products. The solvents were removed under reduced pressure and the residues were purified using column chromatography with *n*-hexane/ethyl acetate (9:1). The product mixtures (pale yellow solid) were then analyzed with chiral HPLC to determine the enantiomeric excesses. Analytics for reaction with H-D-Pro-Pro-Glu-NH_2: **^{1}H-NMR (500 MHz, $CDCl_3$)**: δ (ppm) = 9.72 (d, $J = 2.5$ Hz, 1H, O=C*H*), 7.32 (m, 3H, Ar-*H*), 7.18 (m, 2H, Ar-*H*), 4.72 (dd, $J = 4.9$ Hz, $J = 12.7$ Hz, 1H, NO_2CH_2), 4.63 (dd, $J = 9.8$ Hz, $J = 12.7$ Hz, 1H, NO_2CH_2), 3.79 (dt, $J = 4.9$ Hz, $J = 9.8$ Hz, 1H, ArC*H*), 2.68 (m, 1H, EtC*H*), 1.51 (m, 2H, CH_3CH_2), 0.82 (t, $J = 7.6$ Hz, 3H, CH_2CH_3); **ESI-QMS**: $[M-H]^-$ calculated for $C_{12}H_{15}NO_3$: $m/z = 220.11$; found: $m/z = 220.12$, 221.12.

Batch catalysis

30 mg (0.0051 mmol, 0.001 eq.) of Sil-P10-Cat and 30 mg (0.0030 mmol, 0.001 eq.) of Sil-P30-Cat were reacted each with *n*-butanal (3.00 eq.) and β-nitrostyrene (1.00 eq., 88.18 mg/mL) in $CHCl_3$/*i*-PrOH (9:1) at room temperature for 16 h. After this time, the suspensions were centrifugated, the solvents were separated from the materials and analyzed with UHPLC-ESI-QMS. After removing the solvent under reduced pressure, the residues were purified using column chromatography with *n*-hexane/ethyl acetate (9:1). The product mixtures were then analyzed with chiral HPLC.

Batch recycling

After centrifugation, the particles from the batch catalysis experiments were washed 3 times with $CHCl_3$ and *i*-PrOH, respectively, and then air dried. The catalytic cycle was then repeated twice as described above or with the conditions given in Table 3. Again, the solutions were analyzed by UHPLC-ESI-QMS and chiral HPLC.

Flow catalysis

Heterogeneous Catalysis in flow The flow reactor (either a stainless steel column filled with Sil-P10/30-Cat as packed bed reactor or a functionalized silica monolith) was attached to a HPLC pump and washed with $CHCl_3$/*i*-PrOH (9:1) for 30 min before the catalysis. Afterwards, the reaction solution (0.3 M ß-nitrostyrene solution in $CHCl_3$/*i*-PrOH (9:1) 6 eq. of *n*-butanal) was pumped through the reactor with a flow rate of 0.05 mL min^{-1} at room temperature for 3 to 24 h depending on the cycle. At the given intervals, aliquots were taken of the solution exiting the reactor and analyzed *via* HPLC to determine conversion and enantiomeric excess. After each cycle, the reactor was washed with solvent for 30 min.

Supporting Information

The authors have cited an additional reference within the Supporting Information.[37]

Acknowledgements

R. D. Brand and S. A. Busche have contributed equally to this work, and each has the right to list himself first in bibliographic documents. The authors cordially thank Stefan Bernhardt (JLU Giessen) for the chiral HPLC measurements. Open Access funding enabled and organized by Projekt DEAL.

Conflict of Interests

The authors declare no conflict of interest.

Data Availability Statement

The data that support the findings of this study are available on request from the corresponding author. The data are not publicly available due to privacy restrictions.

Keywords: continuous flow catalysis · mesoporous silica materials · inverse electron-demand Diels-Alder reaction · organocatalysis · supported catalysis

[1] a) S. Mukherjee, *Curr. Sci.* **2021**, *121*, 1148–1151; b) D. W. C. MacMillan, *Nature* **2008**, *455*, 304–308; c) B. List, *Chem. Rev.* **2007**, *107*, 5413–5415; d) B. List, R. A. Lerner, C. F. Barbas, *J. Am. Chem. Soc.* **2000**, *122*, 2395–2396.
[2] a) S. Mukherjee, J. W. Yang, S. Hoffmann, B. List, *Chem. Rev.* **2007**, *107*, 5471–5569; b) E. Juaristi, *Tetrahedron* **2021**, *88*, 132143.
[3] a) A. J. Metrano, A. J. Chinn, C. R. Shugrue, E. A. Stone, B. Kim, S. J. Miller, *Chem. Rev.* **2020**, *120*, 11479–11615; b) C. G. Avila-Ortiz, M. Pérez-Venegas, J. Vargas-Caporali, E. Juaristi, *Tetrahedron Lett.* **2019**, *60*, 1749–1757; c) C. G. Avila-Ortiz, L. Díaz-Corona, E. Jiménez-González, E. Juaristi, *Molecules* **2017**, *22*.
[4] M. Wiesner, M. Neuburger, H. Wennemers, *Chemistry (Weinheim an der Bergstrasse, Germany)* **2009**, *15*, 10103–10109.
[5] M. Wiesner, G. Upert, G. Angelici, H. Wennemers, *J. Am. Chem. Soc.* **2010**, *132*, 6–7.
[6] Y. Arakawa, M. Wiesner, H. Wennemers, *Adv. Synth. Catal.* **2011**, *353*, 1201–1206.
[7] Y. Arakawa, H. Wennemers, *ChemSusChem* **2013**, *6*, 242–245.
[8] a) M. Ferré, R. Pleixats, M. Wong Chi Man, X. Cattoën, *Green Chem.* **2016**, *18*, 881–922; b) J. G. Hernández, E. Juaristi, *Chemical communications (Cambridge, England)* **2012**, *48*, 5396–5409.
[9] B. G. Wang, B. C. Ma, Q. Wang, W. Wang, *Adv. Synth. Catal.* **2010**, *352*, 2923–2928.
[10] a) A. Puglisi, S. Rossi, *Physical Sciences Reviews* **2021**, *6*; b) C. de Risi, O. Bortolini, A. Brandolese, G. Di Carmine, D. Ragno, A. Massi, *React. Chem. Eng.* **2020**, *5*, 1017–1052; c) R. Gérardy, N. Emmanuel, T. Toupy, V.-E. Kassin, N. N. Tshibalonza, M. Schmitz, J.-C. M. Monbaliu, *Eur. J. Org. Chem.* **2018**, *2018*, 2301–2351.
[11] a) A. El Kadib, R. Chimenton, A. Sachse, F. Fajula, A. Galarneau, B. Coq, *Angew. Chem. Int. Ed.* **2009**, *48*, 4969–4972; b) D. Enke, R. Gläser, U. Tallarek, *Chem. Ing. Tech.* **2016**, *88*, 1561–1585; c) C. P. Haas, T. Müllner, R. Kohns, D. Enke, U. Tallarek, *React. Chem. Eng.* **2017**, *2*, 498–511.
[12] K. Nakanishi, N. Soga, *J American Ceramic Society* **1991**, *74*, 2518–2530.

[13] R. Meinusch, R. Ellinghaus, K. Hormann, U. Tallarek, B. M. Smarsly, *Phys. Chem. Chem. Phys.* **2017**, *19*, 14821–14834.
[14] a) J. M. Kohn, J. Riedel, J. Horsch, H. Stephanowitz, H. G. Börner, *Macromol. Rapid Commun.* **2020**, *41*, e1900431; b) S. Arias, S. Amini, J. Horsch, M. Pretzler, A. Rompel, I. Melnyk, D. Sychev, A. Fery, H. G. Börner, *Angew. Chem. Int. Ed.* **2020**, *59*, 18495–18499.
[15] G. S. Scatena, A. F. de la Torre, Q. B. Cass, D. G. Rivera, M. W. Paixão, *ChemCatChem* **2014**, *6*, 3208–3214.
[16] a) B. T. Worrell, J. A. Malik, V. V. Fokin, *Science* **2013**, *340*, 457–460; b) C. P. R. Hackenberger, D. Schwarzer, *Angew. Chem. Int. Ed.* **2008**, *47*, 10030–10074; c) B. D. Fairbanks, D. M. Love, C. N. Bowman, *Macromol. Chem. Phys.* **2017**, *218*, 1700073; d) J. Horsch, P. Wilke, M. Pretzler, M. Seuss, I. Melnyk, D. Remmler, A. Fery, A. Rompel, H. G. Börner, *Angew. Chem.* **2018**, *130*, 15954–15958; e) K. Li, D. Fong, E. Meichsner, A. Adronov, *Chem. Eur. J.* **2021**, *27*, 5057–5073; f) A. Vázquez, R. Dzijak, M. Dračínský, R. Rampmaier, S. J. Siegl, M. Vrabel, *Angew. Chem.* **2017**, *129*, 1354–1357; g) J. C. T. Carlson, H. Mikula, R. Weissleder, *J. Am. Chem. Soc.* **2018**, *140*, 3603–3612; h) G. Moad, E. Rizzardo, S. H. Thang, *Aust. J. Chem.* **2012**, *65*, 985; i) T. Pauloehrl, G. Delaittre, V. Winkler, A. Welle, M. Bruns, H. G. Börner, A. M. Greiner, M. Bastmeyer, C. Barner-Kowollik, *Angew. Chem. Int. Ed.* **2012**, *51*, 1071–1074; j) J.-F. Lutz, H. G. Börner, *Prog. Polym. Sci.* **2008**, *33*, 1–39.
[17] a) X. Ren, A. H. El-Sagheer, T. Brown, *Analyst* **2015**, *140*, 2671–2678; b) E. J. L. Stéen et al., *ACS Nano* **2020**, *14*, 568–584.
[18] a) C. F. Hansell, P. Espeel, M. M. Stamenović, I. A. Barker, A. P. Dove, F. E. Du Prez, R. K. O'Reilly, *J. Am. Chem. Soc.* **2011**, *133*, 13828–13831; b) V. R. Flid, M. L. Gringolts, R. S. Shamsiev, E. S. Finkelshtein, *Russ. Chem. Rev.* **2018**, *87*, 1169–1205; c) J. Schoch, M. Wiessler, A. Jäschke, *J. Am. Chem. Soc.* **2010**, *132*, 8846–8847; d) B. L. Oliveira, Z. Guo, G. J. L. Bernardes, *Chem. Soc. Rev.* **2017**, *46*, 4895–4950; e) A.-C. Knall, C. Slugovc, *Chem. Soc. Rev.* **2013**, *42*, 5131–5142.
[19] S. A. Busche, S. Peplau, L. Zuhse, D. Steimer, D. D. August, H. G. Börner, *Polym. Chem.* **2023**.
[20] a) J. A. Bonham, M. A. Faers, J. S. van Duijneveldt, *Soft Matter* **2014**, *10*, 9384–9398; b) V. K. Sarin, S. B. H. Kent, R. B. Merrifield, *J. Am. Chem. Soc.* **1980**, *102*, 5463–5470.
[21] K. Turke, R. Meinusch, P. Cop, E. Da Prates Costa, R. D. Brand, A. Henss, P. R. Schreiner, B. M. Smarsly, *ACS Omega* **2021**, *6*, 425–437.
[22] J. S. Schulze, R. D. Brand, J. G. C. Hering, L. M. Riegger, P. R. Schreiner, B. M. Smarsly, *ChemCatChem* **2022**, *14*.
[23] Y.-L. Tain, L.-C. Jheng, S. K. C. Chang, Y.-W. Chen, L.-T. Huang, J.-X. Liao, C.-Y. Hou, *Molecules* **2020**, *25*.
[24] H. Jeong, D. Youn, J. Nam, J. Kim, Y.-S. Lee, D.-S. Shin, *Bull. Korean Chem. Soc.* **2018**, *39*, 29–32.
[25] S. Große, P. Wilke, H. G. Börner, *Angew. Chem. Int. Ed.* **2016**, *55*, 11266–11270.
[26] R. Bollhagen, M. Schmiedberger, K. Barlos, E. Grell, *J. Chem. Soc. Chem. Commun.* **1994**, 2559.
[27] G. Linden, L. Zhang, F. Pieck, U. Linne, D. Kosenkov, R. Tonner, O. Vázquez, *Angew. Chem. Int. Ed.* **2019**, *58*, 12868–12873.
[28] C. Yu, L. Qian, M. Uttamchandani, L. Li, S. Q. Yao, *Angew. Chem. Int. Ed.* **2015**, *54*, 10574–10578.
[29] M. Baalmann, M. J. Ziegler, P. Werther, J. Wilhelm, R. Wombacher, *Bioconjugate Chem.* **2019**, *30*, 1405–1414.
[30] M. Vrabel, P. Kölle, K. M. Brunner, M. J. Gattner, V. López-Carrillo, R. de Vivie-Riedle, T. Carell, *Chemistry (Weinheim an der Bergstrasse, Germany)* **2013**, *19*, 13309–13312.
[31] C. Wappl, V. Schallert, C. Slugovc, A.-C. Knall, S. Spirk, *Molecules* **2021**, *26*.
[32] F. Thébault, A. J. Blake, C. Wilson, N. R. Champness, M. Schröder, *New J. Chem.* **2006**, *30*, 1498–1508.
[33] M. Thommes, K. Kaneko, A. V. Neimark, J. P. Olivier, F. Rodriguez-Reinoso, J. Rouquerol, K. S. Sing, *Pure Appl. Chem.* **2015**, *87*, 1051–1069.
[34] P. Werther, J. S. Möhler, R. Wombacher, *Chem. Eur. J.* **2017**, *23*, 18216–18224.
[35] L. J. Alcock, K. D. Farrell, M. T. Akol, G. H. Jones, M. M. Tierney, H. B. Kramer, T. L. Pukala, G. J. Bernardes, M. V. Perkins, J. M. Chalker, *Tetrahedron* **2018**, *74*, 1220–1228.
[36] S. Eissler, M. Kley, D. Bächle, G. Loidl, T. Meier, D. Samson, *J. Pept. Sci.* **2017**, *23*, 757–762.
[37] E. Kaiser, R. L. Colescott, C. D. Bossinger, P. I. Cook, *Anal. Biochem.* **1970**, *34*, 595–598.

Manuscript received: June 22, 2023
Revised manuscript received: July 27, 2023
Accepted manuscript online: August 7, 2023
Version of record online: September 4, 2023